Metastable γ-MnS Hierarchical Architectures: Synthesis, Characterization, and Growth Mechanism

Yuanhui Zheng, Yao Cheng, Yuansheng Wang,* Lihua Zhou, Feng Bao, and Chong Jia

State Key Laboratory of Structural Chemistry, Fujian Institute of Research on the Structure of Matter, Chinese Academy of Sciences, and Graduate School of Chinese Academy of Sciences, Fuzhou, Fujian 350002, China

Received: January 18, 2006; In Final Form: March 8, 2006

Preparation of shape-controlled metastable γ-MnS semiconductor nanocrystals has been achieved on a large scale through a simple solvothermal method in the presence of PVP. The key strategy is the use of sulfur powder as sulfur source in ethylene glycol (EG) solvent that also acted as a weak reducing agent. Reaction parameters such as reaction time and temperature are found to be important in controlling various hierarchical architectures, such as homogeneous semi-hollow core−shell, hollow nanospheres, and nanowires. Transmission electron microscopy observations indicate that these hierarchical architectures are formed mainly via Ostwald ripening. The optical absorption measurements reveal that these novel architectures exhibit remarkable shift of absorption peak during the course of structural compaction and grain growth.

1. Introduction

In past years, there has been extensive interest in synthesis of nanostructures with specific morphologies and properties.[1,2] It is well-known in the literature that inorganic hollow structures (e.g., tubular, spherical, and cagelike) from nano- to microscale may bring a series of opportunities for potential applications in drug delivery, sensors, filters, coatings, and chemical catalysis,[3−9] owing to their unique structural, optical, and electrical characteristics. Recently, many efforts have been devoted to modifying the outer or inner part of hollow architectures or, in other words, increasing the complexity of the hollow structures, which are expected to further enhance the physical and chemical performances and thus enable the materials to meet more needs of technological applications. As an example, CuO and ZnO hollow dandelion-like conformations and ZnS homogeneous core−shell architectures were studied by Liu et al.[10−12] So far, a number of methods have been developed to fabricate hollow structures, with the most versatile one being temperate-directed synthesis. In this case, the surface of a template can be directly coated with a layer of objective products to generate a heterogeneous core−shell structure, and subsequent removal of the template results in hollow structure with controllable dimension and size. In addition to the above common chemical method, a recent development is that some traditional physical phenomena, such as "Kirkendall effect" and "Ostwald ripening", could also be utilized to construct hollow metal oxide/sulfide spheres.[11−15]

As a p-type semiconductor with a wide gap ($E_g \approx 3.7$ eV), manganese sulfide (MnS) can form three kinds of polymorphs such as the rock salt structure (α-MnS), the zinc-blends structure (β-MnS), and the wurzite structure (γ-MnS). It has a potential application in solar cells as a window/buffer material. In addition, it is also linked with the study of diluted magnetic semiconductors (DMS). The interesting magnetic and magneto-optical properties of DMS, which arise from spin-exchange interactions between the dopant ions and the semiconductor charge carriers, have been investigated widely in order to utilize these materials for semiconductor spin-based electronics or spintronics.[16,17] The group II−VI semiconductors of chalcogenide nanocrystals with Mn doping are the typical and the most popular DMS, showing unique magneto-optical properties caused by a strong sp−d exchange interaction between electron/hole band states and Mn^{2+} 3d electron states.[18,19] There is also an anti-ferromagnetic correlation between the Mn^{2+} ($S = {}^5/_2$) spins due to d−p−d super-exchange interaction in these materials.[20,21] Stimulated by these promising applications, much attention has focused on the control of the architectures (morphologies) and crystalline phases of MnS nanocrystals.[22−25] Herein, we report a facile and efficient solvothermal route to synthesize hierarchical architectures of γ-MnS nanocrystals, including homogeneous semi-hollow core−shell, hollow nanospheres, and nanowires. Ethylene glycol (EG) in the reaction acted not only as a solvent but also as a weak reducing agent. An Ostwald ripening growth mechanism for these novel architectures has been discussed in detail. Moreover, the optical absorptions of these materials were measured, and the results exhibit the remarkable shift of absorption peak during the course of structural evolution and related grain growth.

2. Experimental Section

2.1. Synthesis. Manganese acetate, sulfur powder, ethylene glycol (EG), and poly(*N*-vinyl-2-pyrrolidone) (PVP, Mw = 30000) were all of analytical grade and purchased from Shanghai Chemical Reagent Ltd. without further purification. Metastable γ-MnS homogeneous semi-hollow core−shell and hollow nanospheres were synthesized through a facile solvothermal route. In a typical procedure, 0.245 g (1 mmol) of manganese acetate and 0.600 g of PVP (2×10^{-2} mmol, with molar ratio of PVP to manganese salt of 2×10^{-2}:1) were dissolved in 30 mL of EG solvent. The transparent mixture was then put into a Teflon-lined stainless steel autoclave of 70 mL capacity followed by addition of 0.032 g (1 mmol) of sulfur and subsequent agitation. The sealed tank was heated at a rate of 5 °C/min to 190 °C and maintained at this temperature for 0.75−3 h in an oven. After reaction, the autoclave was cooled to room temperature naturally. The resulting precipitates were collected by

* Corresponding author. Tel/Fax: +86-591-8370-5402. E-mail: yswang@fjirsm.ac.cn.

10.1021/jp060351l CCC: $33.50
Published on Web 04/04/2006

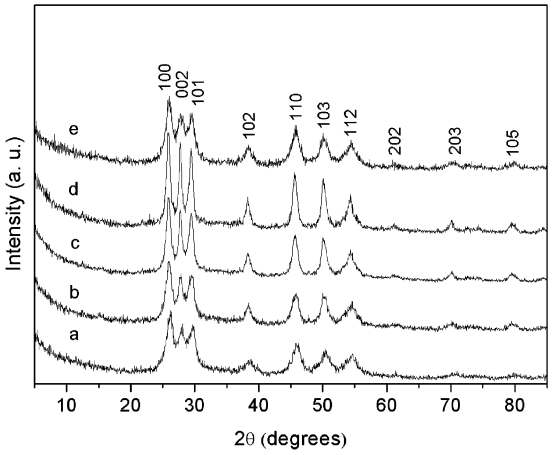

Figure 1. XRD patterns of the colloidal samples synthesized (a−d) at 190 °C for 0.75, 1.5, 2.25, and 3 h, respectively, and (e) at 180 °C for 3 h.

centrifugation, washed with CS_2 and pure ethanol several times, and finally dried in air at room temperature. The γ-MnS nanowires were synthesized in the same way at 180 °C for 3 h.

2.2. Characterizations. Powder X-ray diffraction (XRD) patterns of the samples were recorded by an X-ray diffractometer (RIGAKU-DMAX2500) with Cu Kα radiation ($\lambda = 0.154$ nm) at a scanning rate of 5°/min for 2θ ranging from 5 to 85°. The morphology and microstructure of the as-synthesized sample were characterized by a transmission electron microscope (TEM, JEOL-2010) equipped with an energy-dispersive X-ray spectroscopy (EDS) system and operated at 200 kV, and a field emission scanning electron microscope (SEM, JSM-6700F) working at 10 kV. Optical absorption spectra were recorded on a spectrophotometer (Lambda900, Perkin-Elmer) with a spectral range from 200 to 800 nm and a resolution of 2.0 nm.

3. Results and Discussion

The XRD patterns of the as-prepared samples are shown in Figure 1. All the diffraction peaks on the curves are in good agreement with the standard hexagonal γ-MnS (space group: $P6_3mc$, lattice constants $a = 0.398$ nm, $c = 0.645$ nm (PDF # 40-1289)). No other characteristic peaks of α-MnS and β-MnS were observed. Since no strong reducing agents (e.g., potassium borohydride or hydrazine hydrate) were used in the experiments, it is believed that the EG solvent has been working as a weak reducing agent. The essence of this solvothermal synthesis is the reduction of sulfur powder (S) but not manganese ions (Mn^{2+}) by EG solvent (reduction potential: $E° = 0.14$ V for $S + 2H^+ + 2e \rightarrow H_2S$; $E° = -1.18$ V for $Mn^{2+} + 2e \rightarrow Mn$). Therefore, the chemical reactions are proposed as follows:

$$2HOCH_2{-}CH_2OH = 2CH_3CHO + 2H_2O \quad (1)$$

$$2CH_3CHO + S = CH_3CO{-}COCH_3 + H_2S \quad (2)$$

$$Mn(CH_3COO)_2 + H_2S = MnS(s) + 2CH_3COOH \quad (3)$$

As a simple confirmation of the above reactions, there was an odor of hydrogen sulfide after reaction.

Various hierarchical architectures of γ-MnS nanocrystals were synthesized controllably by adjusting experimental parameters (e.g., reaction time, temperature, and the amount of PVP). A low-magnification SEM image reveals the overall morphology of the sample synthesized at 190 °C for 3 h: uniform nanospheres with a mean diameter of about 500 nm (see Supporting Information SI-1). The TEM observation (Figure 2a) clearly shows the white contrast at the center of these nanospheres with shell thickness ranging from about 100 to 200 nm, suggesting it is hollow inside the nanosphere. A high-magnification SEM image of the γ-MnS nanocrystals (Figure 2b) further confirms the hollow nanosphere morphology. Figure 2c is a magnified TEM image from the edge of a nanosphere, revealing that the γ-MnS spherical shell is comprised of nanorods with widths of about 10 nm. A typical high-resolution TEM (HRTEM) image (Figure 2d) of the nanorods shows uniform lattice structure, free of detectable defects. The corresponding fast Fourier transform (FFT) pattern from the squared region of Figure 2d (inset in Figure 2d) is indexed to hexagonal γ-MnS crystal along the [010] zone axis, indicating that the preferential growth direction of the nanorods is along [001]. However, with a shorter reaction time of 1.5 h, γ-MnS homogeneous semi-hollow core−shell nanospheres were achieved. Unlike the heterogeneous type, homogeneous core−shell structures are in general more difficult to fabricate. Figure 3a shows the interesting semi-hollow homogeneous core−shell structure, which is further confirmed by SEM observation from a cracked nanosphere shown in Figure 3b. It may be noted that most of the nanospheres in Figure 3a are concentric core−shell configurations, while some are basket-like ones (highlighted by the circles). EDS analysis at the center and at the edge of a

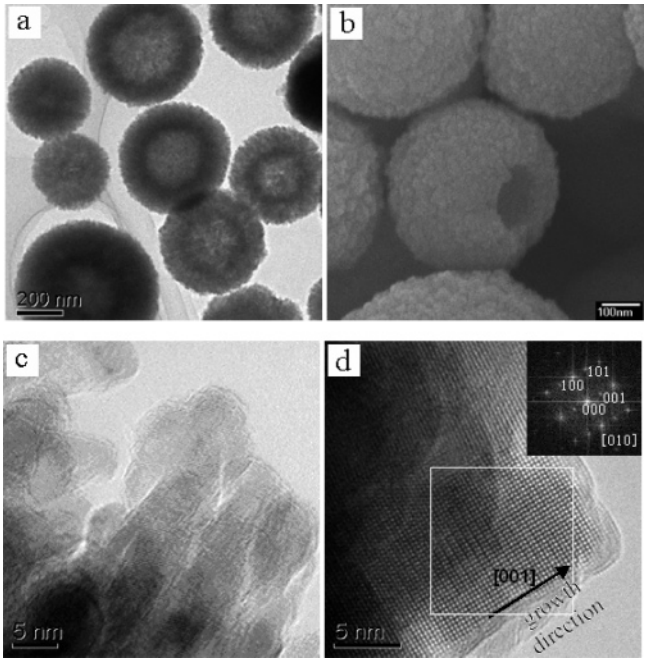

Figure 2. (a) TEM and (b) SEM images of γ-MnS hollow nanospheres, (c) the magnified TEM, and (d) HRTEM images of the edge of a nanosphere synthesized at 190 °C for 3 h.

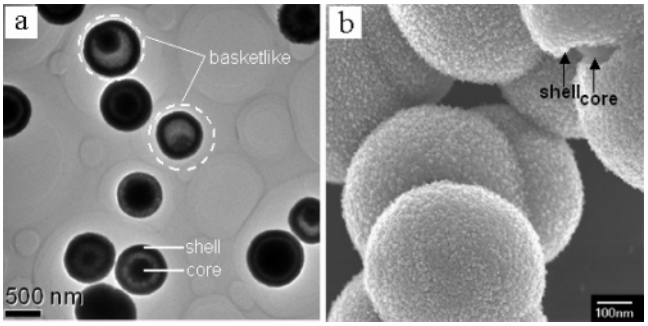

Figure 3. (a) TEM and (b) SEM images of the γ-MnS homogeneous core−shell nanospheres synthesized at 190 °C for 1.5 h.

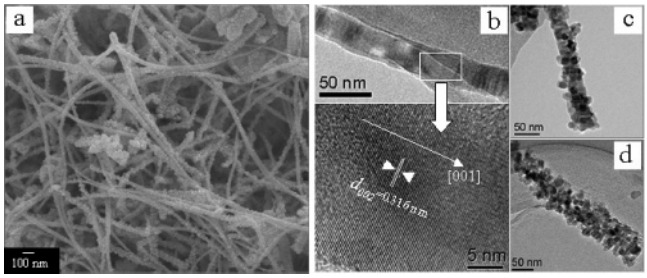

Figure 4. (a) SEM image of the γ-MnS nanowires; (b−d) TEM/HRTEM images of the individual nanowires, showing three types of morphologies. Synthetic condition: 180 °C, 3 h.

nanosphere reveals the stoichiometric composition of MnS (atomic ratio of Mn/S approximates to 1:1, see Supporting Information SI-2), and no oxygen peaks were detected, indicating that there was no oxide layer on the surface of the nanosphere, in good agreement with the above XRD result. The reaction temperature also plays an important role in shape control of the γ-MnS nanocrystals, similar to the result reported by Jun and co-workers.[25] At a higher temperature (190 °C), small primary γ-MnS nanocrystals tended to aggregate together to form 3D nanospheres, as described above. However, at a lower temperature (180 °C) for 3 h, a high yield of ultra-long nanowires with width of about 50 nm were formed, as presented in Figure 4a. Three types of nanowire morphologies could be found, as clearly demonstrated in Figure 4b−d. TEM and HRTEM images of a nanowire with smooth surface (Figure 4b) indicate that it is a single crystal with preferential growth direction along [001]. Figure 4c presents the second type of nanowire consisting of a single-crystalline nanowire in the center and many small nanoparticles attached on its surface. The third type of nanowire is constructed of many small nanoparticles aggregating together without an objective central axis, as shown in Figure 4d. The SAED patterns of the individual nanowires in Figure 4c and 4d (see Supporting Information SI-3) reveal that they are nanoparticulates. Interestingly, after aging for a longer time of 4 h, these nanowires vanished; instead, hollow nanospheres were obtained (see Supporting Information SI-4). A study of the relationship between the ratio of PVP to manganese salt and the parameters (size, structure) of γ-MnS nanospheres reveals that PVP surfactant contributes not only to stabilizing and dispersing the γ-MnS nanospheres but also to controlling the formation of the regular geometry (see Supporting Information SI-5 in detail).

To obtain a better understanding of the formation and evolution of metastable γ-MnS nanocrystals, time-dependent experiments were carried out. The shape evolution of spherical aggregates is shown in Figure 5. It is obvious that, at the early reaction stage (0.75 h), the primary nanocrystallites tended to aggregate together to form 3D solid nanospheres with pale edges and dark centers at higher temperature (e.g., 190 °C), as presented in Figure 5a. At this stage, the exterior of the nanospheres were packed much looser than the interior, indicating the intrinsic density variations inside these starting solid aggregates. When reacted for 1.5 h, the solid evacuation started at a particular region underneath the immediate surface layer, which divided most of the solid spheres into two discrete regions, resulting in the formation of a semi-hollow homogeneous core−shell structure as shown in Figure 5b. When the reaction duration was prolonged to 2.25 h, the single-wall hollow nanosphere and two different types of core−shell nanospheres with a hollow core (double-wall homogeneous core−shell structure) were observed, as displayed in Figure 5c. Finally, after the reaction was further prolonged to 3 h, the cores in the

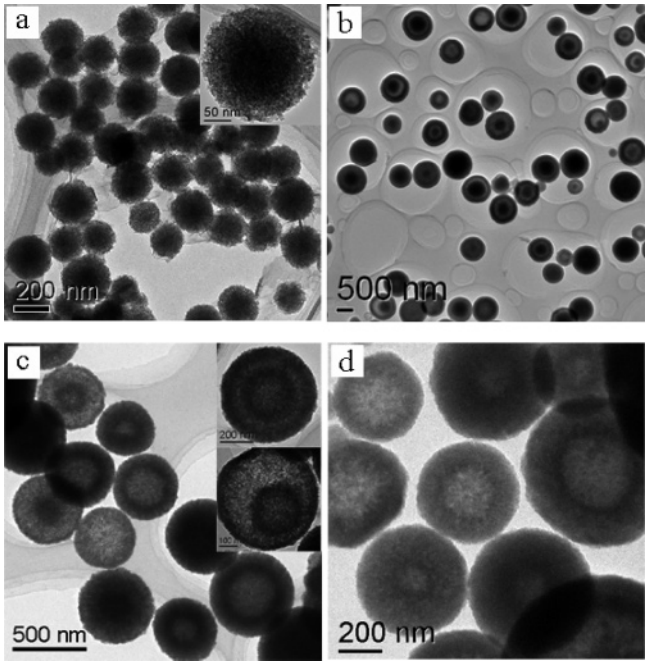

Figure 5. TEM images of the γ-MnS spheres with hierarchical structure synthesized at 190 °C for (a) 0.75 h, (b) 1.5 h, (c) 2.25 h, and (d) 3 h, respectively, in the presence of PVP.

center of most core−shell spheres were evacuated completely, resulting in the single-wall hollow structures, as demonstrated in Figure 5d.

Naturally, a question comes to us: why does the density variation inside the starting solid aggregates occur? We believe that it is related to the formation of H_2S molecules during the sample preparation process. At the early reaction stage, the generated H_2S molecules through reaction 2 would be exhausted immediately by excessive Mn^{2+} ions through reaction 3 to produce γ-MnS primary nanoparticles; thus, only a very small amount of (or even no) H_2S molecules would remain. With the reactions going on, the amount of the remnant H_2S would increase due to the decreasing of Mn^{2+} ions in the system, and these gas molecules would be trapped on the newly formed primary nanoparticles due to the high viscosity of the reactant medium. Since the initially formed primary nanoparticles may aggregate together and then act as the cores for the subsequent aggregation of the new ones, the center region of the starting solid aggregates would be packed more densely than the outer.

Based on the above results, it is believed that Ostwald ripening should be the main formation mechanism for these novel hierarchical architectures. It is well-known that the Ostwald ripening process involves "the growth of larger crystals from those of smaller size which have a higher solubility than the larger ones".[27,28] Figure 6 shows various ripening manners that have been elucidated in detail by Zeng's group[12] and Peng's group.[26] In our synthetic system, it is evident that the formation of γ-MnS hierarchical core−shell and hollow architectures at higher temperature is another example of the symmetric/asymmetric Ostwald ripening, completely different from the template-directed growth where the melting sulfur droplet acts as template for the formation of simple hollow nanostructure reported by Lei et al.[22] The original driving force for this ripening could be attributed to the existence of intrinsic density variations inside the starting solid aggregates. The formation and evolution of nanospheres seem to be as follows: at first, driven by the minimization of the total energy of the system, the small primary γ-MnS nanocrystals aggregated together to

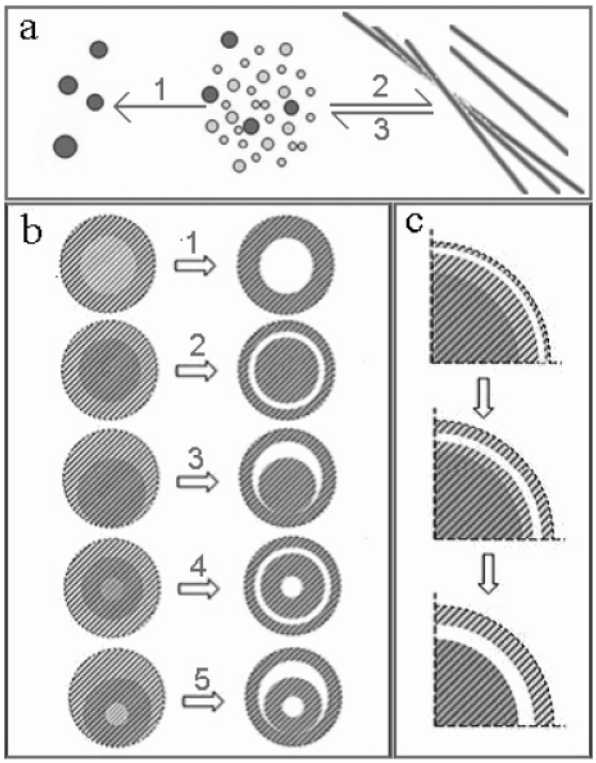

Figure 6. (a) Various schemes of Ostwald ripening for colloidal particles: (1) isotropic ripening, (2) anisotropic ripening, and (3) one-dimension to two-dimension intraparticle ripening (1D to 2D ripening):[26] the dimension of the crystals increased along the short axis and decreased along the long axis with total crystal volume unchanged. (b) Various schemes of Ostwald ripening for spherical aggregates:[12] (1) core hollowing process, (2) symmetric, and (3) asymmetric Ostwald ripening for formation of a homogeneous core−shell structure, (4) a combination of 1 and 2, (5) a combination of 1 and 3; (c) proposed model for the formation of the void space between core and shell in scheme 2 of (b); darker areas: larger and/or closely packed crystallites; lighter areas: smaller and/or loosely packed crystallites; white areas: void space.

form 3D solid nanospheres, which exhibit various packing densities along the radial direction. The outer crystallites packed loosely would serve as starting growth sites for the subsequent recrystallization. As the mass was transported, the void space between the core and the shell was generated mainly through the symmetric ripening. Appearance of some basket-like nanospheres suggests that asymmetric ripening happened as well. The nanorods in the shell were formed via fast recrystallization on the crystallographic planes with high surface energy (anisotropic ripening, scheme 2 of Figure 6a). It is obvious that the cores could further be excavated in a manner presented in schemes 1 of Figure 6b, resulting in double-wall hollow nanospheres. Once the cores in the center of the nanospheres were consumed completely, the final single-wall hollow nanospheres were created. On the other hand, at lower temperature (180 °C) for 3 h, the single-crystalline nanowires (Figure 4b) should be formed through anisotropic ripening (scheme 2 of Figure 6a), while polycrystalline nanowires shown in Figures 4c and 4d were formed via self-assembly of nanocrystals. When the reaction time was prolonged to 4 h, the single-crystalline nanowires could evolve to small nanoparticles via 1D to 2D ripening (scheme 3 of Figure 6a), which agglomerated together immediately to form nanospheres followed by the hollowing process already discussed above.

Figure 7 presents the UV−vis absorption spectra of the γ-MnS hierarchical architectures dispersed in absolute ethanol.

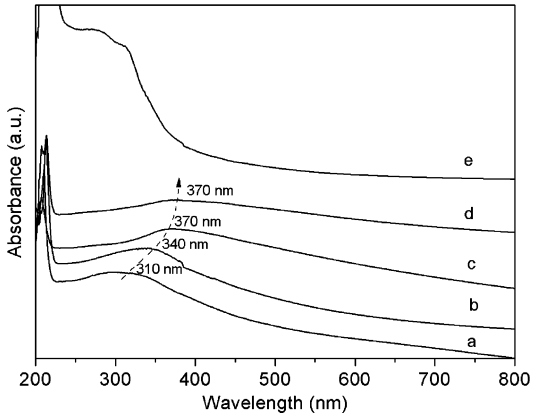

Figure 7. UV−vis absorption spectra of the colloidal samples synthesized (a−d) at 190 °C for 0.75, 1.5, 2.25, and 3 h, respectively, and (e) at 180 °C for 3 h.

The evolution of the absorption peak of the γ-MnS nanospheres is revealed in Figure 7a−d. The direction of the arrow indicates the peak shift during the course of Ostwald ripening. However, the absorption edge of γ-MnS nanowires locates at about 325 nm (Figure 7e), which is almost the same as the value of γ-MnS single-crystalline nanowires reported by others.[24,25] The shift in absorption spectra should be related to the structural evolution (e.g., grain growth) already depicted in Figure 5. More detailed investigation on the optical property of γ-MnS nanocrystals with hierarchical architectures will be carried out in our future work.

4. Conclusions

In summary, various hierarchical architectures of γ-MnS nanocrystals, including homogeneous semi-hollow core−shell, hollow nanospheres, and nanowires, were synthesized through a solvothermal method. It has been demonstrated that these complex nanostructures are controllable by adjusting the reaction time and temperature. The optical absorption measurements of γ-MnS nanospheres displayed remarkable shift of absorption peaks during the course of the structural evolution, indicating that their optical properties could be tuned, which can have potential applications in luminescence fields. It is believed that the results of the present investigation may provide an efficient approach for designing and fabricating a class of group II−VI semiconductor nanomaterials.

Acknowledgment. This work was supported by the project of Nano-molecular Functional Materials of Fujian Province (2005HZ01-1) and the grant of the Natural Science Foundation of Fujian Province (A0320001). Helpful comments by the reviewers are appreciated.

Supporting Information Available: SEM image showing the overall morphology of the nanospheres, figure showing EDS spectra, and table giving the elemental composition of semi-hollow core−shell nanospheres; TEM images of the second and third types of morphologies of nanowires and the SEM and TEM images of γ-MnS nanospheres and nanocrystals. This material is available free of charge via the Internet at http://pubs.acs.org.

References and Notes

(1) Ijima, S. *Nature* **1991**, *354*, 56.
(2) Chopra, N. G.; Luyken, R. J.; Cherrey, K.; Crespi, V. H.; Cohen, M. L.; Louie, S. G.; Zettl, A. *Science* **1995**, *269*, 966.
(3) Caruso, F. *Adv. Mater.* **2001**, *13*, 11.
(4) Dinsmore, A. D.; Hsu, M. F.; Nikolaides, M. G.; Marquez, M.; Bausch, A. R.; Weitz, D. A. *Science* **2002**, *298*, 1006.

(5) Yang, M.; Ma, J.; Zhang, C.; Yang, Z.; Lu, Y. *Angew. Chem., Int. Ed.* **2005**, *44*, 2.
(6) Xu, A.; Yu, Q.; Dong, W.; Antonietti, M.; Cölfen, H. *Adv. Mater.* **2005**, *17*, 2217.
(7) Yang, H. G.; Zeng, H. C. *J. Phys. Chem. B* **2004**, *108*, 3492.
(8) Mayers, B.; Jiang, X.; Sunderiand, D.; Cattle, B.; Xia, Y. *J. Am. Chem. Soc.* **2003**, *125*, 13364.
(9) Chen, J.; Saeki, F.; Wiley: B. J.; Cang, H.; Cobb, M. J.; Li, Z.; Au, L.; Zhang, H.; Kimmey, M. B.; Li, X.; Xia, Y. *Nano Lett.* **2005**, *5*, 273.
(10) Liu, B.; Zeng, H. C. *J. Am. Chem. Soc.* **2004**, *126*, 8124.
(11) Liu, B.; Zeng, H. C. *J. Am. Chem. Soc.* **2004**, *126*, 16744.
(12) Liu, B.; Zeng, H. C. *Small* **2005**, *1*, 566.
(13) Yin, Y.; Rioux, R. M.; Erdonmez, C. K.; Hughes, S.; Somorjai, G. A.; Alivisatos, A. P. *Science* **2004**, *304*, 711.
(14) Yang, H. G.; Zeng, H. C. *J. Phys. Chem. B* **2004**, *108*, 3492.
(15) Chang, Y.; Teo, J. J.; Zeng, H. C. *Langmuir* **2005**, *21*, 1074.
(16) Pearton, S. J.; Abernathy, C. R.; Overberg, M. E.; Thaler, G. T.; Norton, D. P.; Theodoropoulou, N.; Hebard, A. F.; Park, Y. D.; Ren, F.; Kim, J.; Boatner, L. A. *J. Appl. Phys.* **2003**, *93*, 1.
(17) Wolf, S. A.; Awschalom, D. D.; Buhrman, R. A.; Daughton, J. M.; von Molnar, S.; Roukes, M. L.; Chtchelkanova, A. Y.; Treger, D. M. *Science* **2001**, *294*, 1488.
(18) Furdyna, J. K. *J. Appl. Phys.* **1988**, *64*, R29.
(19) Goede, O.; Heimbrodt, W. *Phys. Status Solidi B* **1988**, *146*, 11.
(20) Hass, K. C.; Ehrenreich, H. *J. Cryst. Growth* **1988**, *86*, 8.
(21) Larson, B. E.; Hass, K. C.; Ehrenreich, H.; Carlsson, A. E. *Solid State Commun.* **1985**, *56*, 347.
(22) Lei, S.; Tang, K.; Yang, Q.; Zheng, H. *Eur. J. Inorg. Chem.* **2005**, *20*, 4124.
(23) Biswas, S.; Kar, S.; Chaudhuri, S. *J. Cryst. Growth* **2005**, *284*, 129.
(24) Lu, J.; Qi, P.; Peng, Y.; Meng, Z.; Yang, Z.; Yu, W.; Qian, Y. *Chem. Mater.* **2001**, *13*, 2169.
(25) Jun, Y.; Jung, Y.; Cheon, J. *J. Am. Chem. Soc.* **2002**, *124*, 615.
(26) Peng, Z. A.; Peng, X. *J. Am. Chem. Soc.* **2001**, *123*, 1389.
(27) Ostwald, W. *Z. Phys. Chem.* **1897**, *22*, 289.
(28) Ostwald, W. *Z. Phys. Chem.* **1900**, *34*, 495.